論文 / 著書情報
Article / Book Information

Title	Elongation of extreme ultraviolet (at 13.5 nm) emission with time-of-flight controlled discharges and lateral fuel injection
Authors	Tomonao Hosokai,Takuma Yokoyama,Alexei Zhidkov,Hiroto Sato,Eiki Hotta,Kazuhiko Horioka
Citation	Journal of Applied Physics, Vol. 104, 053306,
発行日/Pub. date	2008, 9
公式ホームページ /Journal home page	http://jap.aip.org/
権利情報/Copyright	Copyright (c) 2008 American Institute of Physics

Elongation of extreme ultraviolet (at 13.5 nm) emission with time-of-flight controlled discharges and lateral fuel injection

Tomonao Hosokai,[1,a)] Takuma Yokoyama,[2] Alexei Zhidkov,[3] Hiroto Sato,[2] Eiki Hotta,[1] and Kazuhiko Horioka[1]
[1]*Department of Energy Sciences, Interdisciplinary Graduate School of Science and Engineering, Tokyo Institute of Technology, 4259 Nagatsuta, Yokohama, Kanagawa 226-8502, Japan*
[2]*Extreme Ultraviolet Lithography System Development Association (EUVA), R&D Center, Gotenba 1-90 Komakado, Gotenba, Shizuoka 412-0038, Japan*
[3]*Central Research Institute of Electric Power Industry, 2-6-1 Nagasaka, Yokosuka, Kanagawa 240-0196, Japan*

(Received 11 April 2008; accepted 1 July 2008; published online 10 September 2008)

A way toward a quasicontinuous extreme ultraviolet (EUV) radiation source is proposed and explored. Tin and lithium vapor discharges with the lateral laser-ablation injection are experimentally studied as possible efficient sources of quasicontinuous emission of EUV radiation at a wavelength of 13.5 nm. It is shown that the time-of-flight control of optimal plasma parameters by means of varying ablating laser pulse parameters provides a considerable elongation of maximal-power EUV emission with an overall efficiency of 0.1% and with an energy output exceeding 1% of the energy deposited in the discharge plasma. Along with a high average power and a stable position, such an emitter may have its size small enough to be used in the projection lithography. © *2008 American Institute of Physics*. [DOI: 10.1063/1.2975211]

I. INTRODUCTION

Kinetics and dynamics of multiple-charged ion plasma, which is the most efficient source of extreme ultraviolet (EUV) radiation, have been extensively studied for the past decade.[1] Plasma of various elements, xenon, tin, lithium, gold, and so on produced by infrared or visible laser pulses or by different types of discharge, has been examined as a possible source with a wavelength of 13.5 nm incoherent radiation.[2–5] Comprehensive analysis has been performed for the ionization physics and radiation transfer.[6] However, the conventional approaches have been shown to be unable to give a source with required characteristics: a high average power with a small size of the source for projection lithography.[7,8]

It has also been shown that at a fixed input power the EUV emission produced by multiply charged ions has a maximum, $P_{\max}$, at an optimal electron density $N_{e,\mathrm{opt}}$ and electron temperature $T_{e,\mathrm{opt}}$:[6] ion recombination or ionization accompanying, for example, a temperature decrease or increase changes the ionization balance with a reduction in line emission. The volume of the emitter, V, is also limited because in the projection technique an incoherent source must be a point source. Therefore, the maximal energy output $E = P_{\max} \times V \times t$, where t is the plasma lifetime, can be reached only with a continuous source.

In conventional EUV sources such as laser-produced plasma,[2] discharge produced plasma (DPP) including plasma focus, and various z-pinches[3–5] based on confined plasma, the optimal condition for the EUV emission is usually maintained for several hundreds of nanoseconds. The condition is broken by either plasma instabilities or by strong electron diffusion or by local plasma dynamics. These negative processes cannot be easily suppressed because the power of plasma radiation for the conditions is too low to control the total plasma energy balance; the use of the blackbody radiation, $\sim T_e^4$, may considerably reduce the efficiency of line radiation due to absorption.[6,9]

Practically so far in the DPP studies, the dynamic compression of fuel gas by z-pinch and vacuum spark discharges with a drive current of few tens of kiloamperes is mainly used for producing the plasma column with the required EUV parameters. In z-pinches, a high temperature and a high density are achieved during the stagnation in its implosion phase. However, plasma expands so rapidly after the stagnation of the column that the optimal temperature and density for the EUV emission can be maintained shortly on the order of submicroseconds.[7] In a vacuum spark exploiting high-density vapors from electrodes, the evaporation process depends on the direct heating by discharge current. It is difficult to maintain the temperature and density of the plasma for the EUV emission for a long time because a fuel supply and a drive current cannot be independently controlled. Even though such schemes can provide quite high conversion efficiency (CE) order of 2%–3%, they fail in the overall efficiency: the total energy of the EUV emission is too low for a practical application. On the other hand, if the proper plasma temperature and density for the EUV emission can be kept quasicontinuously by any discharge scheme it would give a very high average energy of the EUV emission even at a lower CE.

We believe that there is a way to control the plasma energy balance along with the plasma ionization through a continuous evacuation of the overheated plasma from the radiation zone. In an ideal case of a continuous gas jet such an EUV source could also be ceaseless. In the present paper,

a)Electronic mail: hosokai@es.titech.ac.jp.

we demonstrate this by igniting a laser-triggered discharge in laser-ablated-vapor jets with EUV emission with a duration as long as the jet duration.

II. TIME-OF-FLIGHT CONTROL PLASMA

Usually the plasma of an EUV source is characterized by the optimal electron density and temperature. For 1–10 MW input power, which is typical for a discharge, the parameters lie in the range $N_e \sim 10^{19}$ cm^{-3} and $T_e \sim 50$ eV.[6] A temperature increases or decreases as well as a density. A change of the parameters leads to decreases in the useful radiation power, owing to a change of ionization balance in the plasma. The maximal size of the radiating plasma should be less than 1 mm to reduce the divergence of the EUV radiation after its magnification.[7] For these parameters and tin plasma, the time of a three-body recombination[9,10] can be estimated as $\tau_{3B}=[6\times10^{-27}z^3N_e^2T_e^{-9/2}]^{-1}\sim(10^{-8}-10^{-7})$ s, where N_e, T_e, and z are the electron density, the electron temperature, and the ion charge, respectively. For a plasma with a typical size order of 0.1 cm, its dynamics will contribute to the plasma energy balance if the plasma velocity exceeds $V=10^6$ cm/s and the time of flight (the time of fuel crossing a discharge area) is about 10^{-7} s.

Typical plasma balance equations for ion population, N_z, and plasma energy, W, in strongly collisional plasma have the following form:[9]

$$dN_z/dt = S_{z-1}N_eN_{z-1} - (S_z + R_zN_e)N_eN_z + R_{z+1}N_e^2N_{z+1} - N_z/\tau, \tag{1}$$

$$dW/dt = j^2/\sigma + \sum_z E_z^R R_z N_e^2 N_z - \sum_z E_z^{\text{ion}} S_z N_e N_z - Q_{\text{rad}} - Q_{\text{dyn}}, \tag{2}$$

where S_z and R_z are the ionization and recombination rates, τ is the time of the particle evacuation from the discharge area, E_z^R is the energy deposited in the plasma due to recombination of ion z, and E_z^{ion} is the energy loss per ionization act;[9] j and σ are the current density and the plasma conductivity; Q_{rad} and Q_{dyn} are the energy losses due to plasma radiation and due to the particle leaving the plasma bulk. For a constant j and Q_{rad}, Q_{dyn} equal zero, there is no steady state solution of Eqs. (1) and (2) except the full ionization of the plasma. However, the useful EUV radiation can be emitted only by excitation or recombination of particular ions. Plasma radiation can control the plasma temperature and ionization balance if it is close to the blackbody radiation, $\sim T^4$; this regime is far from the optimal for the EUV emission. Nevertheless, plasma dynamics may be a key for the control over plasma energy balance. The energy loss, owing to the plasma dynamics, can be estimated as $Q_{\text{dyn}} \sim (N_eT_e + N_iT_i)/\tau$, where τ is a parameter determined by initial conditions. For the moving plasma, this parameter may be called the time of flight. Since the parameter τ is tunable, there is a value of τ that gives a steady solution of Eqs. (1) and (2) with the maximal power of the EUV emission.

The use of the discharge on gas jets as a source of EUV has been proposed in Ref. 4. A z-pinch discharge was ignited in a xenon gas jet. However, the duration of the EUV radiation was considerably shorter than that of a driving current pulse, and the size of the emitter was several millimeters. The velocity of an atomic jet might be too low for the time-of-flight control. Even in a supersonic gas jet with a high Mach number, the jet velocity is order of 10^5 cm/s that may be not enough to control the energy balance. The velocity can be considerably increased with the use of the expanding plasma. It is apparent that excessive high velocity decreases the plasma temperature and, therefore, may shift the parameters from the ideal.

The simplest method to make a rapidly expanding plasma is the laser ablation. It is well known that if the intensity of nanosecond or subnanosecond laser pulses is much higher than the threshold energy of plasma formation, the jet velocity is determined by the plasma temperature and, even in the case of $M<1$, where M is a Mach number of the jet, can reach $V=10^7$ cm/s.[11,12] However, after the laser pulse, the velocity of the expanding vapor becomes much less.

We estimate the velocity of a laser-ablated-vapor jet in the vicinity of the discharge long after the laser pulse to prove that a laser-triggered discharge can be ignited in the time-of-flight regime via performing a two-dimensional (cylindrical symmetry) hydrodynamic simulation of the metal target ablation by a laser pulse with a wavelength of 1 μm based on the comprehensive model described in Ref. 11, neglecting plasma radiation and meniscus effects.

Following the model, we solve the heat conduction equation for the condense part of the target in a two-dimensional approximation, $\rho_c C_p(\partial T_c/\partial t + V_c \partial T_c/\partial x) = \nabla\cdot(\kappa\nabla T_c)$, where ρ_c and T_c are the density and temperature of the condense matter, V_c is the velocity of the boundary between condense and evaporated parts, and C_p and κ are the specific heat and thermal conductivity and conventional gas-dynamic equations along with the quasi-one-dimensional laser radiation transfer equation.[11] The equations of state for the plasma, $p=p(\mathbf{r},T)$, $\epsilon=\epsilon(\mathbf{r},T)$, are taken as an ideal plasma ($\gamma=5/3$) including the equilibrium plasma ionization (Saha–Boltzmann equation[10]). These equations are accompanied by conventional initial and boundary conditions, including the interface boundary conditions

$$\kappa\,\partial T_c/\partial x = AI + L_v\rho_c V_c, \quad \rho_c V_c = \rho(V_c - v),$$

$$\rho_c V_c^2 = \rho(V_c - v)^2 + P,$$

where L_v is the heat of evaporation and P, v, are ρ are the pressure, velocity, and density of the vapor. Additional relations of temperature and density are taken from Crout model for evaporation.[11,12]

Figure 1 illustrates the dynamics of vapor velocity and vapor density calculated for a tin target nearby a discharge axis that is usually placed several milimeters far from the target. The target is evaporated by a Gaussian-shape laser pulse of 0.5 ns duration focused with $P=40$ J/cm^2 and $P=400$ J/cm^2 with the same spot size. This corresponds to a typically low and to a typically high velocity of ablating vapor injection, respectively, described in Sec. IV A. Despite the large difference in the pulse energies, the vapor density dynamics in both cases are similar. A high temperature

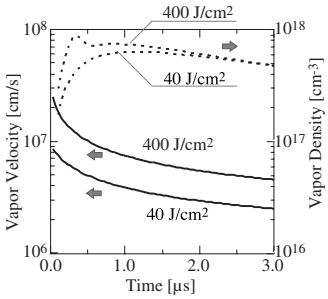

FIG. 1. Calculated dynamics of tin vapor velocity and density on the laser axis at 2 mm far from the plane target irradiated by 40 J/cm^2 and 400 J/cm^2 0.5 ns duration laser pulse. Solid lines and dashed lines indicate the vapor velocity and the vapor density, respectively.

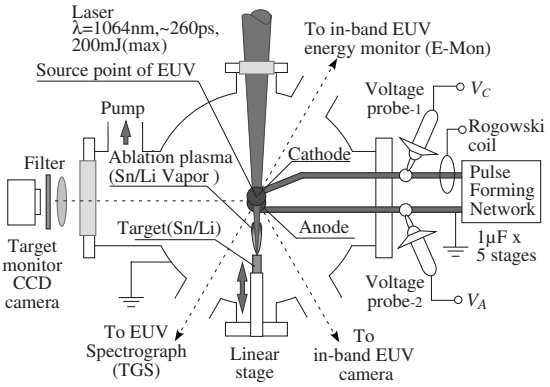

FIG. 2. Experimental setup.

plasma formed near the ablating surface screens the laser light; therefore an essential difference in vapor densities appears in the very beginning of the vapor evolution. In contrast to the vapor density, velocities of the vapor can be changed by an increase in the energy of laser pulses. In both cases the vapor velocities in microsecond time scale much exceed a maximal velocity of a typical gas jet. Although the flight time is longer than the recombination time it may be short enough to control the plasma energy balance and ionization dynamics, making them the steady state. Assuming that the deposition power in the 1 mm^3 volume plasma is $W=1$ MW and the plasma density and temperature are $N_e=10^{19}$ cm^{-3} and $T_e=20$ eV, respectively, one can get from Eqs. (1) and (2) that, to control the plasma balance, the time of flight should be about $\tau \sim W/(l^3 N_e T_e)=3\times 10^{-8}$ s or velocity $V=l/\tau=3\times 10^6$ cm/s. Such a velocity can be achieved in the laser-ablated plasma as it follows from the simulations. The low temperature (in the long period, the vapor temperature is much lower than the EUV optimal temperature and has no effect on the EUV emission efficiency) of the atom vapor expends and may become a fuel for the long discharge. The vapor density does not change with the ablating pulse energy, while the vapor velocity does. It is apparent that a too high vapor velocity may result negatively; by varying the laser pulse energy one can match plasma conditions to optimize the EUV emission.

A maximal time of a vapor jet in the simulation is about 10 μs that allows, in general, production of a quasicontinuous vapor jet with 10–100 kHz lasers. Theoretically, such a system would consume 10 MW power for discharge and 2–5 kW of the laser energy and generate an EUV output order of 100 kW. A proper off-duty factor makes the system practical.

In the present paper, we investigate the EUV emission from laser-triggered discharges ignited in laser-ablated tin and lithium vapor jets that cross an electrode axis. The EUV emission at a wavelength of 13.5 nm from tin and lithium plasmas and its dependence on the time-of-flight control is measured and analyzed. We demonstrate the ability of the time-of-flight control of discharge parameters leading to considerable elongation of the EUV emission.

III. EXPERIMENTAL SETUP

In the experiment, characteristics of the EUV emission are studied in discharges generated in ablated vapors produced from a solid target irradiated by laser pulses and injected into the gap between the discharge electrodes. Figure 2 illustrates a typical experimental setup: a vacuum chamber, electrodes, EUV detectors, and a laser-ablated target. A pair of electrodes is set at the central axis inside the vacuum chamber, where the source plasma for the EUV emission is produced. A pulse-forming network (PFN) charged to $U=-5$ kV is connected to the electrodes. The five staged PFN consisting of five capacitors of 1.0 μF and proper inductors produces a discharge current with a tapered-top waveform. A total current of the circuit is monitored by a Rogowski coil; the electrical potentials of terminals connecting to the electrodes are measured by high-voltage probes that set outside the vacuum chamber. The detectors, the in-band EUV energy monitor, the transmission-grating spectrograph (TGS) for EUV, the in-band EUV camera, and the solid target on the linear stage are arranged transversely with respect to the electrode axis. The surface conditions of the electrodes and the target are monitored by the charge coupled device (CCD) camera in the direction of 90° from the laser axis. Figure 3 illustrates a cross-sectional view of the electrodes and the target region corresponding to the image by the target monitor CCD camera. The electrodes consist of a needle-cathode made from a sharpened rod of 1.2 mm in diameter and a boll anode of 10.0 mm in diameter, which are coaxially arranged in the axis. They are made of tungsten. The two ring-shape permanent magnets (with an outer diameter of 100 mm, an inner bore of 20 mm, a thickness of 15 mm, and the distance between the two magnets of 20 mm) are set coaxially in the axis, making a uniform magnetic field in the discharge region

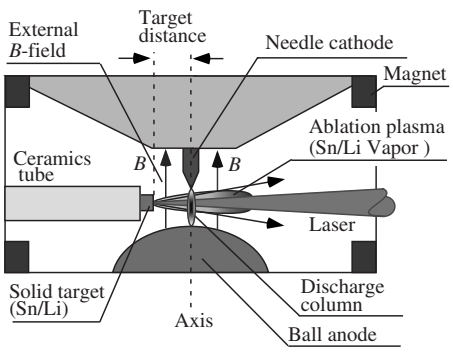

FIG. 3. Side view of the electrodes and the target region.

in the axis direction with $B=0.1$ T. This magnetic field is preserved for more complex injection schemes. The distance between the top of the needle cathode and the surface of the ball anode is 2 mm.

A laser target as a vapor source is set outside the discharge area in the direction of 90° from the electrode axis. The solid tin (Sn) or lithium (Li) is chosen as the target material for efficient EUV emission at a wavelength of 13.5 nm. The target is a rod of 100 mm length and of 2 mm diameter for tin (Sn) or 3 mm diameter for lithium (Li). The targets are laminated by a ceramics tube insulator to avoid the electrical breakdown on the target surface. The distance between the target surface and the electrode axis is varied from 1.0 to 10.0 mm to regulate the vapor with proper density into the discharge. The laser axis is 1 mm from the surface of the boll anode. The surface of the cathode and anode is covered with a thin layer of the target material (tin or lithium) as a pretreatment prior to discharges with the use of the vapor deposition of ablation from the target.

The neodymium-doped yttrium aluminum garnet laser system (EKSPLA, SL312) generates up to 200 mJ, 260 ps laser pulses at the fundamental wavelength of 1064 nm with 10 Hz repetition rate. The repetition rate is reduced to a single shot on demand by a mechanical shutter. A laser pulse with a diameter of 8 mm is delivered into the vacuum chamber through the window and is focused on the surface of the target (tin or lithium) with a convex lens of $f=500$ mm. The focus spot size is approximately 300 μm in full width at $1/e^2$ of maximum. The maximum laser intensity on the target is estimated to be order of 1 TW/cm^2.

A laser pulse ablates the fuel vapor and triggers the discharge of the circuit. Because the envelope of laser pulses grazes the periphery of the high-voltage cathode surface, it induces electrical breakdown between the electrodes. The distribution of the vapor jet at the target region is monitored by a filtered time-gated (~10 ms) visible CCD camera. The optical filter cuts the laser light in front of the CCD camera.

An in-band EUV energy monitor (E-Mon, JENOPTIK Mikrotechnik GmbH) consists of a zirconium filter, two multilayer mirrors, and a biased photodiode sensitive in the EUV range and is designed to measure EUV pulses at a central wavelength of 13.5 nm with a bandwidth of 2%. It has a window of 8.0×8.0 mm^2 at the central axis of the discharge region. A TGS for EUV (TGS, AIXUV GmbH) consists of a zirconium filter, a transmission grating with 10 000 lines/mm, and a time-gated (~10 ms) backilluminated CCD camera sensitive in the EUV range. In the experiment, the spectral range of 11.5–17.0 nm is chosen. The signals are calibrated by diffraction efficiency of the grating and by sensitivity of the backilluminated CCD for the wavelengths. The minimum spectral resolution is approximately $\lambda/\Delta\lambda=165$. An EUV in-band camera, which can measure plasma images in the 13.5 nm central wavelength with a bandwidth of 2%, consists of 100 μm pinhole, a zirconium filter, two multilayer mirrors, and a time-gated (~10 ms) backilluminated CCD camera sensitive in the EUV range. The spatial resolution of the camera is limited by the size of the pinhole. In order to avoid damage of the sensitive detectors (the E-mon, the TGS, and the EUV in-band camera) by debris including energetic neutrals and charged particles from the plasma and melting plumes from the electrodes, helium gas flows the path through the front of the filters as a buffer. However, a background pressure of the vacuum chamber is kept lower than 1.0×10^{-4} Torr using turbomolecular pumps. In order to evaluate a net energy input from the discharge into the plasma, a total inductance of the circuit is measured using a dummy load instead of the plasma load.

IV. RESULTS AND DISCUSSION

We measured the EUV emission that changes the target materials, the energy of ablating laser pulses, and the distance between the target surface and the discharge axis (see Fig. 3). It is apparent that the density of the vapor decreases with the distance from the target while with the laser intensity the vapor velocity and density increase. Since the plasma recombination is very sensitive to electron density, we expect a strong dependency of the time-of-flight control not only on the vapor velocity but also on the vapor density. In this paper, the in-band EUV means EUV at a central wavelength of 13.5 nm with a bandwidth of 2%.

A. Tin target experiment

In Figs. 4(a)–4(c) the circuit current I and the net voltage between the electrodes U are given for the charging voltage of the PFN $U_c=-5$ kV and for the tin vapor along with the in-band EUV signal for different energies of the ablating laser pulse. The net voltage between the electrodes U is calculated by the relation $U=V_C-V_A-LdI/dt$, where V_C and V_A are the electrical potentials of the cathode and anode measured by the voltage probes, respectively, and L (~850 nH) is the total inductance of the external circuit obtained with a dummy load. The discharge input power between the electrodes $P=I\times U$ is shown in Fig. 4. The total energy stored in the PFN is 62.5 J. However, the energy of ~30 J is deposited in the discharge; about half of the stored energy are reflected back to the PFN during the total discharge. The laser pulse energy varies as follows: 160 mJ [Fig. 4(a)], 65 mJ [Fig. 4(b)], and 14 mJ [Fig. 4(c)]. The minimal energy of laser pulses is limited by the discharge triggering. We observe no discharge with the pulse energy below 14 mJ. It does not mean that this energy is optimal for the time-of-flight regime with lateral fuel injection. The distance between the target and the discharge axis is 4.5 mm. The discharge current has a tapered rectangular waveform. It increases to 6 kA in ~1.5 μs and from 6 kA to a peak of 8 kA in ~3.3 μs. One can see that the discharge power P does not change significantly with the laser pulse energy even though the density and velocity of the vapor must be changed. In contrast, the dynamics of the in-band EUV signal drastically changes with a decrease in the ablating laser pulse energy and with a corresponding decrease in the fuel vapor velocity. According to the calculation discussed above, the vapor density does not change much with the energy of the laser pulse. Conditionally we may recognize two regimes: high velocity and low velocity of the tin vapor injection. The in-band EUV emission is observed only inside the area during the first half cycle of the discharge current. In all

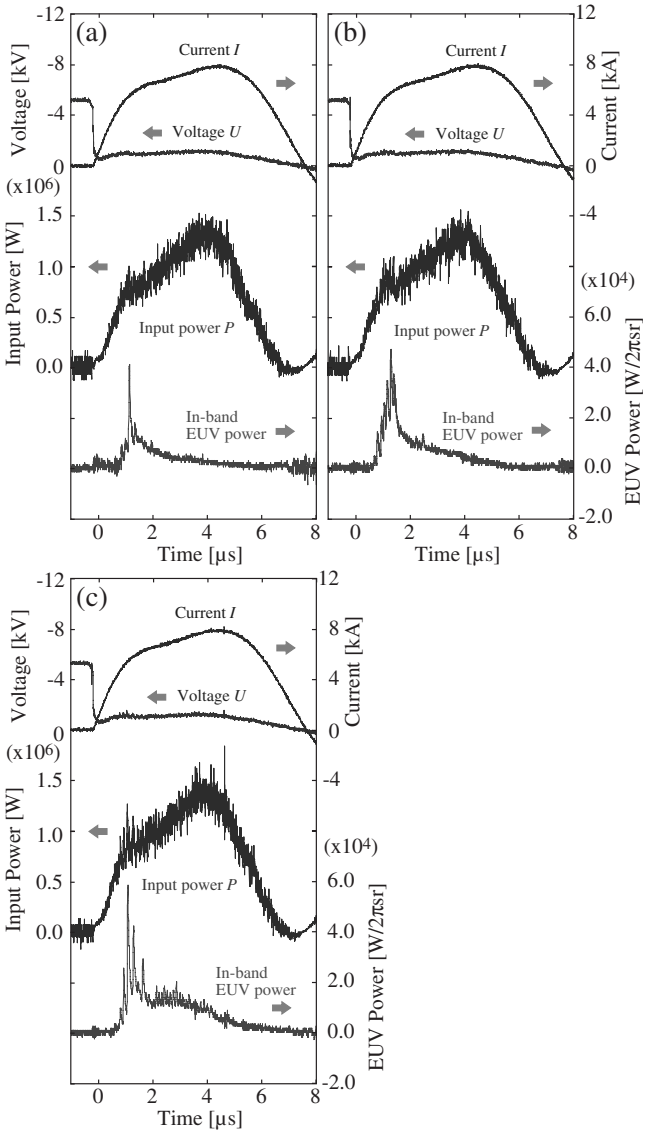

FIG. 4. The current, voltage, input power, and in-band EUV signal in the tin vapor discharge for different energy laser pulses: (a) 160 mJ, (b) 65 mJ, and (c) 14 mJ.

cases, the deposited energy between the electrodes is estimated to be only ~5.6 J in the first half cycle of the discharge current. We regard this value as the energy deposited in the plasma to estimate the CE of the EUV emission since the energy deposited in the electrodes cannot be excluded.

In the case of the high-velocity tin vapor injection corresponding to the highest energy of the ablating laser pulse (160 mJ), one can see a quite short, about 200 ns, peaky in-band EUV signal [see Fig. 4(a)]. The in-band EUV signal appears at 0.7 μs and has a spiky peak at 1.1 μs. The total energy of the in-band EUV emission is estimated to be 25.3 mJ/2π sr. The in-band EUV emission efficiency is ~0.04% of the stored energy in the capacitors or ~0.45% of the energy deposited in the plasma for the first half cycle of the discharge current. We attribute this in-band EUV signal to emission from the vacuum arc discharge ignited by the same laser pulse from the tin-coated electrodes (according to the calculation the drifting vapor cannot reach the discharge region by the rising time of the in-band EUV signal). The

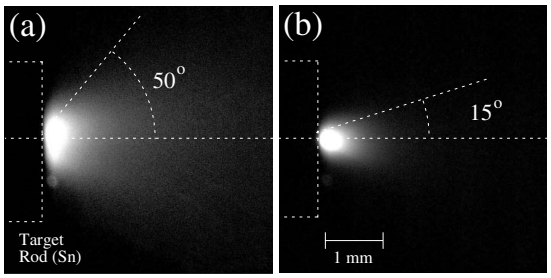

FIG. 5. Visible images (10 ms gate) of the ablated tin plasma plume: (a) fresh surface and (b) after 30 shots. The energy of laser pulses is 100 mJ, and the focusing diameter is 300 μm.

time of flight in this case is small: the plasma rapidly leaves the discharge area that results in a lower plasma temperature. The conditions of the EUV emission with the vapor coming from the target become far from the optimal; therefore no further emission is observed. An interesting fact is that the in-band EUV emission initially does not exist during several shots of the laser in this regime. Initially, there is no tin coat of the electrodes; therefore there is no vacuum arc discharge with the EUV emission. However, after several shots, the dynamics of the vapor dramatically changes. Figure 5 shows typical images of the ablating vapor generated by 100 mJ, 260 ps laser pulses from the fresh target surface [shown in Fig. 5(a)] and after 30 shots [shown in Fig. 5(b)]. The target rod, laser axis, and ejection angle of the jet are illustrated by dashed lines in Fig. 5. One can see an essential change of the vapor plum shape after several shots. Initially the vapor expands in approximately 100° solid angle, while after several shots the angle becomes much smaller, less than 30°, with a considerable increase in the tin vapor density at the discharge axis. This effect appears due to a cavity formation on the tin surface. The cavity depth after several tens of shots is about 1.5 mm while its width is only 0.5 mm. A simple cumulating makes a jetlike structure of the vapor. We have to note that the in-band EUV signal is detected for a while even if we stop the laser ablation. The absence of the vapor jet does not change the EUV signal; it has the shape and amplitude as that shown in Fig. 4. It proves that in the higher velocity regime, the jet serves only for electrode coating and the discharge is the vacuum arc type.

In the case of the intermediate energy of the laser pulse (65 mJ), we observe an elongation of the EUV emission [see Fig. 4(b)]. The total energy of the in-band EUV emission is estimated to be 40.1 mJ/2π sr. The in-band EUV emission efficiency is ~0.07% of the stored energy in the capacitors or ~0.72% of the energy deposited in the plasma for the first half cycle of the discharge current. With a further decrease in the laser pulse energy (14 mJ) and a corresponding decrease in the vapor velocity, we observe additional, much longer, about 5 μs, in-band emission along with the emission from the vacuum arc discharge [see Fig. 4(c)]. This emission comes from the time-of-flight controlled discharge in the ablated tin vapor, and it has a peak at t=3 μs. For the 14 mJ laser pulse, the energy of the in-band EUV emission from the ablating jet more than two times exceeds that emitted from the vacuum arc discharge. The total energy of the in-band EUV emission is estimated to be 59.6 mJ/2π sr. The in-

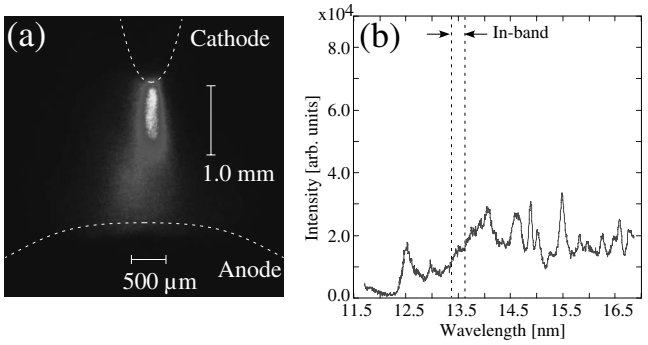

FIG. 6. In-band image of the (a) discharge tin plasma and (b) EUV spectra for laser pulse energy $E=160$ mJ.

band EUV emission efficiency is ~0.1% of the stored energy in the capacitors or ~1.1% of the energy deposited in the plasma for the first half cycle of the discharge current. The emission in this case is still not optimal. A further decrease in the time of flight may result in a better EUV emission. However, if the ablation is stopped, after many shots it corresponds to zero jet velocity of the infinite time of flight, we observe only the vacuum arc discharge with quite short emission. A decrease in the vapor velocity to the gas-jet threshold can be achieved with the coaxial injection (which is discussed in our future paper); in this limit the long EUV emission disappears as well, converting to two short peaks with a much lower power.

The in-band images of the plasma and plasma spectrum near 13.5 nm are given for the laser pulse energy of 160 mJ in Fig. 6 and for 14 mJ in Fig. 7, respectively. They correspond to the signals presented in Figs. 4(a) and 4(c), respectively. Again, one can see an essential difference in the regimes. In the case of the higher vapor velocity, the plasma column is formed for 1–2 μs from the beginning of the discharge [see Fig. 4(a)]. The in-band EUV emission concentrates near the electrode; the bright column has ~1 mm length and ~500 μm diameter [see Fig. 6(a)]. The EUV emission spectrum around the in-band range measured by the TGS (which gives spectral distribution of the EUV emission from the discharge column; the in-band EUV range is illustrated by dashed lines) shows that the relative intensity of 13.5 nm radiation is very small, as shown in Fig. 6(b). The recombination processes shift the ion distribution to low charges with a longer wavelength radiation in this case. For

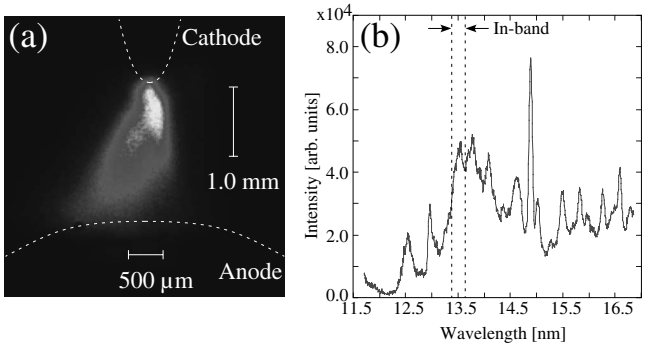

FIG. 7. In-band image of the (a) discharge tin plasma and (b) EUV spectra for laser pulse energy $E=14$ mJ.

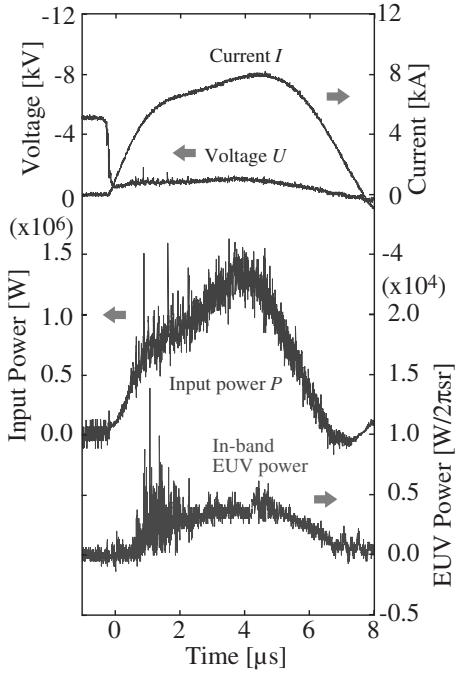

FIG. 8. The current, voltage, input power, and in-band EUV signal in the lithium vapor discharge for 14 mJ energy laser pulse.

the lower vapor velocity case, as shown in Fig. 7, we detected a considerably better spectrum [see Fig. 7(b)]. It indicates that the plasma condition is closer to the optimal. In the in-band plasma image, as shown in Fig. 7(a), the clear sign of the time-of-flight controlled discharge is seen as a backside emitting plasma. The sizes of the plasma are ~1 mm in length and ~500 μm in diameter for the brighter column and are 1 mm in length and ~800 μm in width for the bright cloud region. The shape of the EUV signal in the case of 14 mJ laser pulse is slightly distorted. However, only 15% of the EUV energy comes from the rear of the column, while the total energy increases three times. With the change of the cathode shape to a ball-like, the shape of the bright column remains the same that reflects the time-of-flight character of the emission. The efficiency of the EUV emission in this case drastically reduced.

B. Lithium target experiment

Experiments with the lithium target qualitatively display the same dependencies in the EUV emission. However, the quantitative results are very different. This difference appears because the range of the optimal parameters of the EUV emission for lithium is much broader than that for tin.

Figures 8 and 9 show results of measurements for the Li target, set at 4.5 mm far from the discharge axis and irradiated by 14 mJ energy laser pulses. The electrodes coated by the lithium ablation and the target surface modification by several laser shots are also crucial, similar to the tin target case. The circuit current driven by the PFN, the net voltage between the electrodes, and the discharge power shown in Fig. 8 are quantitatively similar to that of the tin plasma even though the plasma conductivity of the lithium plasma at the same electron temperature should be three to four times as high as that of the tin plasma [$\sigma=1.5\times10^{14}T^{3/2}/(\Lambda\langle z\rangle)$,

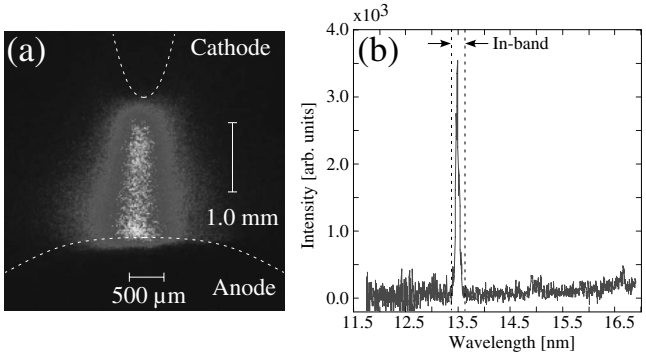

FIG. 9. The (a) in-band image and (b) spectrum in the lithium vapor discharge for 14 mJ energy laser pulse.

where Λ is the Coulomb logarithm and $\langle z \rangle$ is the average ion charge] in the range of the optimal EUV emission, owing to the difference in the charge of radiating ions. This reflects the fact that in both vapors the energy deposited in the plasma is much less than the total energy of the discharge, less than 10%.

Similar to the tin plasma, an in-band EUV signal appears at 0.7 μs with a lot of spiky peaks and its intensity increases with the discharge current. The emission signal lasts for ~6 μs over the half cycle of the discharge. The total energy of the in-band EUV emission is estimated as 18.8 $\text{mJ}/2\pi$ sr for 14 mJ energy of the ablating laser pulse. The in-band EUV emission efficiency is ~0.03% of the stored energy in the capacitors or ~0.34% of the energy deposited in the plasma for the first half cycle of the discharge current. The plasma image obtained by the in-band camera is shown in Fig. 9(a). A bright and straight plasma column with the uniform in-band EUV emission is produced over the area between the electrodes. The size of the bright column is ~2 mm in length and ~1 mm in diameter. The EUV spectrum around the in-band is shown in Fig. 9(b). Because in the case of lithium the strongest emission is an emission of the resonance line of the Li^{2+} ion in both recombination and ionization regimes, the spectrum has a very narrow structure at a wavelength of 13.5 nm corresponding to $2p-1s$ transition of hydrogenlike lithium. The satellite lines of this transition lay out of the in-band. The ratio of the background radiation to the peak intensity in the experiment is better than 5%.

V. CONCLUSION

We have performed measurements of the in-band EUV emission from laser-triggered discharges ignited in laser-ablated tin or lithium vapors with the lateral fuel injection. We have shown that the optimal plasma parameters such as electron temperature and density can be formed and maintained for a longer time. The radiation time can be as long as a duration of a vapor jet (order of several microseconds in the present experiment) by choosing a proper energy of ablating laser pulses and, correspondingly, a proper velocity of the vapor. We called this regime as the time-of-flight control. The time-of-flight control requires a quite high mean velocity of the fuel vapor that cannot be achieved in conventional gas jets. For the highest fuel velocity the laser-ablated plasma has been shown to be a good candidate for the technique. This let us move toward a production of quasicontinuous EUV sources with a high average power.

We have found a very similar behavior of the in-band EUV emission for both tin and lithium vapors. For higher fuel velocities achieved at the highest energy of the ablating laser pulse, discharges in both targets are the vacuum arc type. In this case, the recombination time considerably exceeds the time of flight, and plasma parameters are close to the optimal only for a short time; the EUV emission exists for a short time as well. The maximal efficiency (CE) is about 0.45% of the energy deposited in the plasma. With a decrease in the laser pulse energy and lowering of the vapor velocity, we have observed the time-of-flight control discharges with the longer, several microseconds, in-band EUV emission. The efficiency is considerably increased up to 1.1% of the energy deposited in the plasma. We anticipate that this is not the maximal efficiency of such kind of discharges; according to our estimation, the efficiency can be increased up to 1% of the total energy in capacitors by varying the time of flight.

We have also found that the lithium plasma spectrum is much cleaner than that of the tin plasma. This is apparently due to the contribution of the single line in the in-band range. Therefore the lithium plasma may be a better candidate as a source target.

Another advantage of time-of-flight controlled discharges is much better tolerance to high repetition rate regimes. Because of a low total radiation power in the case of discharges, the input energy remains inside the plasma and can critically heat electrodes even in a few shots. In the time-of-flight control regime this energy can be completely removed from the discharge area due to a high lateral velocity of the plasma.

ACKNOWLEDGMENTS

We are grateful to all members of EUVA R&D Center Gotenba, K. Seki, A. Moriwaki, and T. Igarashi of USHIO Inc. for their encouragements, helpful discussions, and technical support. T.H. strongly acknowledges Dr. A. Yamazaki of the University of Tokyo for his helpful discussions and technical assistance. This research is partly supported by New Energy and Industrial Technology Development Organization (NEDO).

[1]R. Service, Science **293**, 785 (2001).
[2]T. Higashiguchi, C. Rajyaguru, S. Kubodera, W. Sasaki, N. Yugami, T. Kikuchi, S. Kawata, and A. Andreev, Appl. Phys. Lett. **86**, 231502 (2005); Y. Ueno, T. Ariga, G. Soumagne, T. Higashiguchi, S. Kubodera, I. Pogorelsky, I. Pavlishin, D. Stolyarov, M. Babzien, K. Kusche, and V. Yakimenko, *ibid.* **90**, 191503 (2007); T. Higashiguchi, K. Kawasaki, W. Sasaki, and S. Kubodera, *ibid.* **88**, 161502 (2006); T. Higashiguchi, N. Dojyo, M. Hamada, W. Sasaki, and S. Kubodera, *ibid.* **88**, 201503 (2006); S. Namba, H. Nishimura, Y. Yasuda, K. Nagai, N. Miyanaga, Y. Izawa, K. Mima, and K. Takiyama, *ibid.* **88**, 171503 (2006).
[3]V. M. Borisov, A. Yu. Vinokhodov, A. S. Ivanov, Yu. B. Kiryukhin, S. V. Mironov, V. A. Mishchenko, A. V. Prokof'ev, and O. B. Khristoforov, Plasma Phys. Rep. **28**, 877 (2002).
[4]S. R. Mohanty, T. Sakamoto, Y. Kobayashi, N. Izuka, N. Kishi, I. Song, M. Watanabe, T. Kawamura, A. Okino, K. Horioka, and E. Hotta, Appl. Phys. Lett. **89**, 041502 (2006).
[5]M. W. McGeoch, Proc. SPIE **3997**, 861 (2000); W. Partlo, I. Fomenkov,

R. Oliver, and D. Brix, *ibid.* **3997**, 136 (2000); M. A. Klosner and W. T. Silfast, Appl. Opt. **39**, 3678 (2000).
[6]M. Masnavi, M. Nakajima, A. Sasaki, E. Hotta, and K. Horioka, Appl. Phys. Lett. **89**, 031503 (2006); M. Masnavi, M. Nakajima, E. Hotta, K. Horioka, G. Niimi, and A. Sasaki, J. Appl. Phys. **101**, 033306 (2007).
[7]*EUV Sources for Lithography*, edited by V. Bakshi (SPIE, Bellingham, WA, 2006).
[8]K. N. Koshelev, V. I. Balykin, Yu. E. Losovik, and A. Popov, Phys. Usp. **177**, 777 (2007).
[9]V. Derzhiev, A. Zhidkov, and S. Yakovlenko, *Ion Radiation in Non- Equilibrium Dense Plasma* (Energoatomizdat, Moscow, 1986).
[10]Ya.B. Zeldovich, and Yu. P. Raizer, *Physics of Shock Waves and High-Temperature Hydrodynamics Phenomena* (Academic, New York, 1967), Vols. 1 and 2.
[11]V. I. Mazhukin, V. V. Nosov, and I. Smurov, J. Appl. Phys. **101**, 024922 (2007).
[12]B. Wu and Y. C. Shin, J. Appl. Phys. **99**, 084310 (2006); A. V. Gusarov and I. Smurov, *ibid.* **97**, 014307 (2005); A. Miotello and R. Kelly, Appl. Phys. Lett. **67**, 3535 (1995); S. Laville, F. Vidal, T. W. Johnston, O. Barthélemy, M. Chaker, B. Le Drogoff, J. Margot, and M. Sabsabi, Phys. Rev. E **66**, 066415 (2002).